Published in final edited form as:
Mol Immunol. 2007 February ; 44(5): 763–773. doi:10.1016/j.molimm.2006.04.010.

Mutagenesis, biochemical, and biophysical characterization of *Mycoplasma arthritidis*-derived mitogen

Hongmin Li[a,b,*], **Yiwei Zhao**[a,1], **Yi Guo**[a], **Sandra J. VanVranken**[a], **Zhong Li**[a], **Leslie Eisele**[a], and **Walid Mourad**[c]

[a]Wadsworth Center, New York State Department of Health, Empire State Plaza, PO Box 509, Albany, NY 12201-0509, United States

[b]Department of Biomedical Sciences, School of Public Health, University at Albany, State University of New York, Empire State Plaza, PO Box 509, Albany, NY 12201-0509, United States

[c]Université de Montreal, CHUM, Campus St-Luc, PEA, 264, Boul. René Lévesque Est, Bureau 313, Montréal, Qué. H2X 1P1, Canada

Abstract

Mycoplasma arthritidis -derived mitogen (MAM) is a superantigen (SAg) that can activate large fractions of T cells bearing particular TCR Vβ elements. Here we report the mutagenesis, biochemical and biophysical studies on the dimerization of MAM in solution. Our studies showed that although MAM mainly exists as a monomer in solution, a small percentage of MAM molecules form homodimer at high protein concentration, regardless of the presence of Zn^{2+}. A distinct peak corresponding to a MAM homodimer was detected in the presence of EDTA, using both chemical cross-linking and analytical ultracentrifugation methods. Further mutagenesis studies revealed that single mutation of residues at the interface of the crystallographic dimer of MAM does not significantly affect the dimerization of MAM in solution. Circular dichroism (CD) analysis indicated that addition of Zn^{2+} does not induce conformational changes of MAM from its apo-state. Thermal denaturation experiments indicated that addition of Zn^{2+} to MAM solution resulted in a decrease of melting point (T_m), whereas addition of EDTA did not affect the T_m of MAM. These results imply that there is no defined Zn^{2+}-binding site on MAM.

Keywords

MAM; Superantigen; Dimerization; Analytical ultracentrifugation; Sedimentation; Cross-linking; CD

1. Introduction

Mycoplasma arthritidis, a member of the eubacterial class Mollicutes, produces a soluble immunoregulatory factor called *Mycoplasma arthritidis*-derived mitogen (MAM) (Knudtson et al., 1997). MAM functions as a conventional superantigen (SAg) that is characterized by the ability to stimulate the activation of a large fraction of T lymphocytes through simultaneous interactions with class II major histocompatibility complex (MHC) molecules and T-cell receptors (TCR) bearing specific Vβ subsets (Knudtson et al., 1997; Sawitzke et

*Corresponding author. Tel.: +1 518 486 9154; fax: +1 518 474 7992. lih@wadsworth.org (H. Li).
[1]Present address: Department of Biological Chemistry and Molecular Pharmacology, Harvard Medical School, 250 Longwood Ave., Boston, MA 02115, United States.

al., 2000). SAg-induced T-cell activation usually results in the massive release of cytokines, followed by the eventual disappearance or inactivation of responding T cells (Li et al., 1999). Due to their unique features and biological effects, SAgs have been hypothesized to play a role in a number of human diseases, including food poisoning, toxic shock syndrome, scalded skin syndrome, psoriasis, atopic dermatitis, and autoimmune diseases such as Kawasaki syndrome, insulin-dependent diabetes mellitus, multiple sclerosis, and rheumatoid arthritis (Abe et al., 1992; Conrad et al., 1994; Gemmell et al., 1998; Kotzin et al., 1993; Renno and Acha-Orbea, 1996).

The protein sequence of MAM does not exhibit significant global homology to that of any other SAg (Cole et al., 1996; Knudtson et al., 1997). The crystal structures have been determined for more than a dozen bacterial SAgs (Acharya et al., 1994; Arcus et al., 2002, 2000; Donadini et al., 2004; Hakansson et al., 2000; Li et al., 1999; Papageorgiou et al., 1995, 1999; Prasad et al., 1993; Roussel et al., 1997; Schad et al., 1997; Sundberg and Jardetzky, 1999; Sundberg et al., 2002; Sundstrom et al., 1996; Swaminathan et al., 1992; Zhao et al., 2004a). Most staphylococcal and streptococcal pyrogenic SAgs have a similar three-dimensional structure consisting of a small β-barrel domain and a large domain with a β-grasp motif (Li et al., 1999). This is consistent with the fact that these pyrogenic SAgs show high sequence homology with one another (20–98%) (Kim and Schlievert, 1997; Mitchell et al., 2000; Sundberg et al., 2002).

In order to begin to elucidate the structural basis of T-cell activation by this unique SAg MAM, we previously determined the three-dimensional structure of MAM complexed with a human class II MHC molecule, HLA-DR1, loaded with haemagglutinin peptide 306–318 (HA) (Zhao et al., 2004a). The structure indicated that MAM binds predominantly to the MHC α1 domain and the bound HA peptide, and to a lesser extend to the MHC β1 domain (Zhao et al., 2004a). The crystal structure also showed that MAM adopts a novel fold composed of two completely α-helical domains (Zhao et al., 2004a). This fold is entirely different from that of the pyrogenic SAgs. Recently, the crystal and solution structures of another bacterial SAg, *Yersinia pseudotuberculosis* mitogen (YPM), were determined (Donadini et al., 2004). YPM has a single domain composed nearly entirely of β-sheet, showing a jelly-roll-like feature. The structural diversity of these SAgs implies that SAgs of different origins adopt completely different three-dimensional structures, even though they carry out similar biological functions.

Although the crystal structure of MAM in complex with one of its receptors has been determined (Zhao et al., 2004a), a number of biochemical and biophysical characteristics such as thermal dynamic properties remain unknown. In addition, there is discrepancy regarding whether Zn^{2+} is involved in MAM dimerization (Langlois et al., 2003; Zhao et al., 2004a). It has been proposed that dimerization or oligomerization of the MHC antigens by SAgs is critical for both T-cell activation and T-cell-independent cytokine expression on various human antigen-presenting cells (APCs) (Mehindate et al., 1995). The crystal structure of the MAM/HLA-DR1/HA complex revealed that MAM forms a homodimer that cross-links two MHC class II molecules, forming a dimerized SAg-MHC complex (Zhao et al., 2004a).

In order to better understand the function of this potent mitogen, we performed mutagenesis, biochemical and biophysical studies on the dimerization of MAM in solution. Our results show that MAM can form a homodimer at high protein concentration in solution, regardless of the presence or absence of Zn^{2+}. A distinct peak corresponding to the MAM homodimer was detected in the presence of EDTA, using both chemical cross-linking and analytical ultracentrifugation (AUC) methods. Further mutagenesis studies revealed that single mutation of residues at the interface of the crystallographic dimer of MAM does not

significantly affect the dimerization of MAM in solution. Circular dichroism (CD) analysis indicated that the addition of Zn^{2+} does not induce conformational changes of MAM from its apo-state. Thermal denaturation experiments further indicated that Zn^{2+} does not stabilize the MAM structure, implying that there is no defined Zn^{2+}-binding site on MAM.

2. Materials and methods

2.1. Site-directed mutagenesis

Expression plasmid pWM.25B in pGEX-6P-1 vector encoding the wild-type MAM has been described (Langlois et al., 2000). Alanine-scanning mutagenesis was used to individually mutate selected MAM residues at the interface of the crystallographic MAM homodimer (Zhao et al., 2004a). These residues include Leu50, His58, Arg154, Arg192, Tyr193, Tyr194, Glu195, Asp197, and Lys201. The MAM mutants were constructed by using the QuickChange site-directed mutagenesis kit (Stratagene). Nine pairs of primers were designed (data not shown). All mutations were confirmed by DNA sequencing.

2.2. Expression and purification of recombinant proteins

Recombinant wild-type and mutant MAM proteins were expressed as GST-fusion proteins, and were purified as described previously (Langlois et al., 2000; Zhao et al., 2004b).

2.3. SDS-PAGE analysis of MAM dimerization

The cross-linking agent disuccinimidyl glutarate (DSG) (Pierce) was dissolved at a stock concentration of 10 mM in dry DMSO prior to coupling with the proteins. Cross-linking reactions were set up for the recombinant MAM molecule at 3 μM concentration, in 25 μl of a buffer containing 20 mM HEPES, pH 8.0, and 150 mM NaCl. DSG was added to a final concentration of 1 mM. In order to investigate the role of Zn^{2+} in MAM dimerization, we incubated the samples for 1 h in the presence of 30 μM $Zn(OAc)_2$, 300 μM $Zn(OAc)_2$, 30 μM EDTA, or buffer alone. Reactions were stopped with SDS sample buffer, boiled, and separated by electrophoresis in a 12% Tris/glycine acrylamide gel. The separated proteins were then stained with Coomassie blue.

2.4. Analytical ultracentrifugation

Sedimentation velocity (SV) experiments were done at 20 °C in a Beckman Optima XL-I analytical ultracentrifuge at a rotor speed of 55,000 r.p.m. (An50Ti rotor). Double-sector cells were loaded with 400 μl of protein at various concentrations of MAM wild-type (MAM_{wt}) or each MAM mutant, in various buffers. MAM_{wt} was first characterized by SV AUC at concentrations of 11, 25, and 52 μM in a phosphate buffer (buffer A) containing 0.1 M sodium potassium phosphate, pH 6.2, 0.2 M NaCl. Then, SV AUC experiments were performed for MAM_{wt} at 62 μM in citrate buffer (0.1 M citrate, pH 6.2, 0.2 M NaCl), at 55 μM in HBS buffer (10 mM HEPES, pH 7.4, 0.15 M NaCl), or at 55 μM in Tris-HCl buffer (10 mM Tris-HCl, pH 8.0, 0.1 M NaCl). Additional SV experiments were performed for MAM_{wt}, in buffer A, at 27 μM in the presence of 2 mM $ZnCl_2$, or at 25 μM in the presence of 5 mM EDTA. The SV experiments were also performed in buffer A at concentrations of 59, 70, 70, 50, and 42 μM for the MAM mutants I50A, R154A, R192A, E195A, and K201A, respectively. All SV AUC data were recorded with absorbance detection at wavelengths of 280, 294, and 300 nm, for low, moderate, and high concentrations of proteins, respectively. Absorbance fringe displacement profiles were analyzed with the software SEDFIT (http://www.analyticalultracentrifugation.com/) (Vistica et al., 2004), using a model for continuous sedimentation coefficient distributions $c(s)$ (Schuck et al., 2002).

Sedimentation equilibrium studies for MAM_{wt} and mutant MAM molecules were conducted at a temperature of 20 °C and at each of three rotor speeds, 20,000, 25,000, and 30,000 rpm. 100 μl of protein was loaded into Epon double-sector centerpieces at various concentrations in buffer A. For MAM_{wt}, three concentrations, 5, 10, and 50 μM, were used. At least two concentrations were used for five of the MAM mutants: I50 A (13, 20, 43, and 56 μM); R154A (20 and 70 μM); R192A (20 and 70 μM); E195A (14 and 41 μM); and K201A (7, 12, 39 μM). Equilibrium absorbance profiles were acquired at 280, 294, or 300-nm wavelength, depending on the protein concentration. The equilibrium sedimentation data were analyzed using the software SEDPHAT (http://www.analyticalultracentrifugation.com/) (Vistica et al., 2004). Data analysis was performed by global least-squares analysis of data from multiple concentrations and multiple rotor speeds, based on the well known superposition of the Boltzmann distributions of ideal species in the centrifugal field, using conservation of mass constraints (Vistica et al., 2004).

2.5. Circular dichroism

CD spectra of MAM_{wt} at 6.4 μM in HBS buffer, or in HBS buffer supplemented with 1 mM EDTA or $ZnCl_2$, were measured on a J-720 Jasco spectropolarimeter (Japan Spectroscopic Co.) equipped with a temperature-controlled cell holder. Static measurements were recorded at 20 °C. CD spectra were measured at a bandwidth of 1 nm for the far-UV (190–260 nm) using a quartz cell of path length 0.2 mm, and for the near-UV (250–350 nm) using a 1-cm quartz cell. Data from four scans were averaged using the J-720 operating software. Far-UV CD spectra were smoothed by using the Jasco noise reduction routine. The extent of secondary structure of MAM was calculated from the CD spectra in the far-UV spectral range, using the CDPro program suite (Sreerama and Woody, 2000).

The thermal denaturations were carried out for MAM_{wt} at 6.4 μM in HBS buffer, or in HBS buffer supplemented with 1 mM EDTA or $ZnCl_2$, by measurement of the CD ellipticity at 222 nm, with a quartz cell of path length 5 mm. A scan rate of 1 °C/min and a response time of 2 s. were used. The midpoint (T_m) of the heat denaturation was calculated by simulating the experimental melting curve using the protein denaturation routine in the Spectra Analysis software of the Jasco Spectra Manager suite. All the CD experiments were repeated several times, similar results were obtained.

3. Results

3.1. Detection of the MAM homodimer by chemical cross-linking

It was reported that the superantigenic activity of MAM *via* MHC class II molecules is Zn^{2+} dependent, and that Zn^{2+} may trigger the dimerization of MAM (Bernatchez et al., 1997; Etongue-Mayer et al., 2002; Langlois et al., 2003). However, in the crystal structure of the dimerized MAM/HLA-DR1/HA complex (Zhao et al., 2004a), we could not detect Zn^{2+} ion at either the interface of the MAM/HLA-DR1 complex or at the interface of the MAM homodimer, even though the crystallization buffer contained 1 mM $Zn(OAc)_2$ (Zhao et al., 2004a,b). In order to better understand the role of zinc in the biological activity of MAM, we used chemical cross-linking to detect the MAM homodimer in the presence of Zn^{2+} or EDTA. An NHS-ester cross-linker, DSG, can create a covalent amide bond when the DSG conjugation reagent reacts with the amino groups of two molecules in close proximity. This approach is feasible because plenty of amino groups from two molecules in the crystallographic MAM dimer (Zhao et al., 2004a) are close enough for cross-linking. For instance, the side-chain Nζ of Lys49 of one MAM monomer is only 4.5 Å away from Nζ of Lys147 of the other monomer. In addition, the side-chain amino groups of Arg154 of one MAM molecule are within 3.5 Å from the side-chain amino groups of Arg192 of the other MAM molecule in the dimer.

As shown in Fig. 1A, it is obvious that the SDS-PAGE profiles are very similar for the MAM samples treated with 10- or 100-fold excess of $ZnCl_2$, 10-fold excess of EDTA, or buffer alone. Upon cross-linking with DSG, bands corresponding to a MAM homodimer (~50 kDa) in the SDS-PAGE analysis were detected in all four experiments, while native MAM showed only a single band at about 25 kDa (Fig. 1, lane 2). In addition, a band corresponding to a species with a molecular mass of 75 kDa was also detected in each experiment. This band may represent a trimer form of the MAM molecule. The SDS-PAGE analysis indicates that MAM can form a dimer, or even a trimer in solution, regardless of the presence or absence of zinc.

3.2. Analysis of MAM dimerization by sedimentation velocity

Because results obtained from chemical cross-linking may be not conclusive, due to chemical modification of proteins, verification of our results required additional experimental supports. To further characterize MAM dimerization, we performed SV AUC experiments on MAM under various buffer conditions in the presence or absence of Zn^{2+}, using a Beckman XL-1 analytical ultracentrifuge. Due to technical advances and software improvements, AUC has become a powerful tool with which to investigate the oligomerization state of proteins and protein complexes (Dam et al., 2003; Guan et al., 2004; Lebowitz et al., 2002; Schuck et al., 2002). Through monitoring of the sedimentation of a macromolecule in the centrifugal field, its hydrodynamic and thermodynamic properties can be characterized in solution, with the macromolecule in its native state.

Because a MAM homodimer was observed in the asymmetric unit cell in the crystal structure of the MAM/HLA-DR1/HA complex (Zhao et al., 2004a), we initially performed the SV experiment for the wild-type MAM molecule (MAM_{wt}) in a phosphate buffer (0.1 M sodium potassium phosphate, pH 6.2, 0.2M NaCl) that was similar to the buffer used for protein crystallization (Zhao et al., 2004b). As shown in Fig. 2A, the sedimentation coefficient ($S_{(20,w)}$) distribution of MAM at a concentration of 11 μM (~0.3 mg/ml) displayed a single peak, at 2.0 S, corresponding to the monomeric form of MAM. In contrast, the $S_{(20,w)}$ for MAM at a higher protein concentration, 25 μM, showed two distinct peaks, at 2.0 S and at 3.0 S. A $S_{(20,w)}$ of 3.0 is very close to the $S_{(20,w)}$ value (3.1 S) theoretically predicted by hydrodynamic modeling of a MAM dimer, thus implying that MAM forms a dimer in solution. We next increased the protein concentration to 52 μM. High protein concentration apparently promoted dimer formation, resulting in an overall increase of the proportion of the MAM dimer (Fig. 2A). This shift strongly implies that dimer formation for MAM is concentration-dependent, which is consistent with a self-association behavior. In addition, such dimer formation is non-covalent; since MAM contains no cysteine residues, it can not form a disulfide bond-linked homodimer. Therefore, we concluded that non-covalently associated MAM dimer exists in solution.

Because our results thus far were all obtained from the phosphate buffer system at pH 6.2, we next investigated whether MAM dimerization is affected by variations in buffer and pH. Citrate, Tris-HCl, and HEPES buffers, ranging in pH from 6.2 to 8.0, were selected for SV. At high protein concentrations, one peak in the $S_{(20,w)}$ distribution, 2.0 S, was obtained for MAM under each of these buffer conditions (Fig. 2B). A small additional peak at 3.1 S can be identified for MAM in the citrate buffer. Under the conditions with the HEPES or the Tris buffers, the peak near 3.1 S is discerned as a broad shoulder, similar to that observed under the phosphate buffer condition. Nevertheless, although the shapes of the $S_{(20,w)}$ peaks at 3.1 S are different for different buffers, the $S_{(20,w)}$ peaks at 3.1 S for MAM under these diverse conditions each represent the dimer form of MAM. These experiments imply that the dimerization of MAM is not dependent on a particular buffer system.

To further investigate the self-association of MAM, we pre-incubated the protein sample with at least 20-fold excess of EDTA or $ZnCl_2$ (Materials and methods). The samples were then examined by SV. As shown in Fig. 2A, the $S_{(20,w)}$ distribution of MAM in the presence of EDTA showed two peaks similar to those observed for MAM in the absence of EDTA, implying that the addition of the metal-chelator EDTA did not abolish the dimerization of MAM. This indicated that the dimerization of MAM does not require the participation of metal ions such as Zn^{2+}. In agreement with this hypothesis, pre-incubation of MAM with Zn^{2+} did not significantly change the $S_{(20,w)}$ distribution of MAM in the SV experiment. The resultant $S_{(20,w)}$ distribution is very similar to that for MAM in the absence of Zn^{2+} (Fig. 2B).

From all of these SV experiments, over a range of protein concentrations, and under various buffer and pH conditions, and with or without Zn^{2+}, the $S_{(20,w)}$ distribution clearly showed that no peak higher than that (3.1 S) for the MAM dimer was observed. Thus, we found no evidence that a trimer form of MAM exists in solution. It is possible that the higher oligomer state exists but could not be detected under our experimental conditions. Nevertheless, the SV data indicated that MAM can dimerize, independent of Zn^{2+}, over a range of buffer conditions.

3.3. Mutagenesis of MAM residues that are at the interface of the crystallographic MAM homodimer

At the dimer interface in the crystal of the MAM/HLA-DR1/HA complex (Zhao et al., 2004a), the C-terminal domain of one MAM molecule fits into a V-shaped pocket between the N- and C-terminal domains of the other MAM molecule. There are a total of 24 residues from both molecules involved in the dimer interface.

In order to investigate whether the observed crystallographic dimer of MAM corresponds to the MAM dimer in solution, we chose nine amino acids for alanine-scanning mutagenesis, and we investigated the ability of the mutant proteins to dimerize. These residues are Leu50, His58, Arg154, Arg192, Tyr193, Tyr194, Glu195, Asp197, and Lys201. They were selected because of their relatively large contributions to the total buried surface area and to the hydrogen-bonding network, upon MAM dimerization (Zhao et al., 2004a). Each of these amino acids was changed to an alanine using a QuickChange mutagenesis kit (Stratagene). The sequences of all alanine mutants were verified. Expression tests of these mutants indicated that the yields of four mutants, namely H58A, Y193A, Y194A, and D197A, were too low to be suitable for further analysis, whereas the other five mutants, namely L50A, R154A, R192A, E195A, and K201A, had comparable yields to that of the wild-type MAM. The quality of purified MAM mutants was shown in Fig. 1B.

Following protein purification, we performed SV experiments for the latter five MAM mutants. As shown in Fig. 2C, two $S_{(20,w)}$ peaks, corresponding to the monomeric and dimeric forms of MAM, can be detected for each of these mutants by SV, indicating that single mutation to alanine at these sites may not have significant effects on the dimerization of MAM.

To confirm the results obtained from the SV experiments, we performed sedimentation equilibrium studies for the wild-type and mutant MAM molecules, at various protein concentrations, and at three rotor speeds (Fig. 3). The sedimentation equilibrium experiment is an efficient AUC method for measuring the dissociation constant (K_D) for a protein that reversibly self-associates to form oligomers. Using a reversible monomer-dimer model with a global analysis of the equilibrium data (Schuck et al., 2002), we estimated a dissociation constant (K_D) of 1.4 mM with an r.m.s.d of 0.004 for a weak monomer-dimer association of MAM_{wt}. Using the same procedure, the dissociation constants were estimated for the MAM

mutants L50A (2.3 mM), R154A (1.5 mM), R192A (2.3 mM), E195A (1.2 mM), and K201A (1.5 mM). Clearly, the R154A, E195A, and K201A mutations have no effects on MAM dimerization, while the L50A and R192A mutations only resulted in a 1.6-fold reduction in K_D compared to MAM_{wt}. However, because of the very weak self-association, with a K_D value in the millimolar range, such small differences in K_D could result from systematic errors due to instrumental limitations (Schuck et al., 2002). Alternatively, it is possible that L50 and R192 play a minimal role, or no role, in MAM dimerization. Nevertheless, our experiment demonstrated that the selected five MAM residues, when mutated singly to alanines, do not significantly affect the dissociation constants for the monomer-dimer association of mutant MAM molecules. This implies that these individual mutations each have little effect on MAM dimerization.

3.4. CD spectra analysis of MAM

To further characterize MAM and the potential role of zinc in MAM function, we measured the CD spectra for wild-type MAM in apo-state (apo-MAM), and when treated with excess of either EDTA or Zn^{2+} (designated as MAM_{EDTA} and MAM_{Zn}, respectively) (Fig. 4). The shapes and amplitudes of the far-UV CD spectra are characteristic of proteins with a high percentage of helical structure (Fig. 4A). Small differences in the spectral range between 205 and 225 are observed upon addition of excess EDTA or Zn^{2+}. The large differences in the spectra below 200 nm can be attributed to the greater noise level due to the high absorbance of the protein solution in this spectral range. It should be noted that the magnitudes of the far-UV spectra changes for MAM under excess EDTA and Zn^{2+} conditions, relative to the spectra for apo-MAM, are similar. Consistent with this finding, we found that the secondary structural content of MAM_{EDTA}, estimated using the CDPro suite (Sreerama and Woody, 2000), is nearly identical (within 1%) to that of MAM_{Zn}, despite the differences in the measured CD spectra.

In addition to the far-UV CD spectra, which monitor a protein's secondary structural content, we also measured the near-UV (250–350 nm) CD spectra, which can be used to monitor a protein's tertiary structure in the vicinity of the aromatic amino acid residues Tyr, Trp, and Phe (Adler et al., 1973). The near-UV CD spectrum can be sensitive to small changes in tertiary structure due to protein-protein interactions and/or changes in solvent conditions. Signal changes in the near-UV range can be attributed to alterations to Phe (250–270 nm), Tyr (270–290 nm), and Trp (280–300 nm). As shown in Fig. 4B, the near-UV CD spectra of apo-MAM, MAM_{EDTA}, and MAM_{Zn} are very similar. Although subtle differences are evident among the near-UV spectra, they are within systematic error ranges. Thus, we concluded that no conformational alterations to aromatic residues are associated with Zn^{2+} addition, although conformational changes of other non-aromatic residues can not be ruled out.

To examine the thermal stability of MAM under HBS buffer, EDTA, or Zn^{2+} conditions, we performed thermal denaturation experiments, by monitoring secondary structural changes at 222 nm using CD spectra (Fig. 4C). The denaturation experiment indicated that the thermal denaturation of the MAM molecule is an irreversible process. Using the JASCO Spectra Analysis software, we calculated thermal denaturation (melting) midpoint values (T_m) as 48.4 ± 0.07, 48.7 ± 0.25, 43.7 ± 0.12 °C for apo-MAM, MAM with 1 mM EDTA, and MAM with 1 mM Zn^{2+}, respectively. Obviously, the T_ms for apo-MAM and MAM with EDTA are statistically identical, whereas addition of 1 mM Zn^{2+} to MAM solution resulted in a large T_m decrease of about 4.7 °C. These results imply that Zn^{2+} does not stabilize, but rather destabilizes, the MAM structure. It is possible that certain MAM residues that are normally buried were exposed during the thermal denaturation process, resulting in reactions with Zn^{2+} and leading to increased structural disruption.

4. Discussion

It is well established that metal ions, Zn^{2+} in particular, play an important role in the biological function of certain SAgs (Etongue-Mayer et al., 2002; Hudson et al., 1995; Kozono et al., 1995; Langlois et al., 2003; Li et al., 1999, 2001). Zinc may regulate the SAg activity in several ways. First, the metal ion may be directly involved in the interactions between SAgs and their host receptors (Li et al., 1999, 2001; Petersson et al., 2001). Such interactions result in a so-called “high-affinity” SAg-binding site, via a zinc bridge, on the MHC class II molecules (Hudson et al., 1995; Kozono et al., 1995; Li et al., 2001; Petersson et al., 2001). Second, some SAgs can form zinc-dependent homodimers, which could in turn cause dimerization of the MHC class II molecules on the APC surface (Al-Daccak et al., 1998; Baker et al., 2004a,b; Li et al., 1997; Papageorgiou et al., 1995, 2004; Roussel et al., 1997; Sundstrom et al., 1996). Third, zinc may indirectly participate in the interactions between SAgs and host receptors, by inducing conformational changes in certain SAgs; such changes could facilitate the binding of such SAgs to their receptors. Although direct evidence to support this hypothesis is lacking, comparisons of crystal structures of several SAgs with/without Zn^{2+} indeed revealed that there are conformational changes associated with Zn^{2+} binding (Baker et al., 2004a; Hakansson et al., 2000; Papageorgiou et al., 2004). In addition, although there is currently no evidence to support the following possibility, zinc could be required for interactions with co-stimulatory receptors for T-cell activation. Lastly, zinc could induce dimerization of host receptors such as class II MHC molecules, which may enhance the binding of SAgs.

MAM is unique among known SAgs, with a structural fold distinct from those of all other SAgs that have been structurally characterized (Zhao et al., 2004a). Recent studies suggested that MAM superantigenic activity is Zn^{2+} dependent (Bernatchez et al., 1997; Driessen et al., 1995; Etongue-Mayer et al., 2002; Langlois et al., 2003). MAM can induce cytokine gene expression on a human monocytic cell line, THP-1 (Bernatchez et al., 1997). In contrast, stimulation of EDTA-treated THP-1 cells with MAM did not yield any significant cytokine gene expression. Addition of Zn^{2+} restored cytokine gene expression of EDTA-treated THP-1 cells, upon MAM stimulation (Bernatchez et al., 1997). Functional studies further demonstrated that MAM binding to cells of a class II MHC-expressing B cell line, LG2, is Zn^{2+} dependent (Etongue-Mayer et al., 2002). The zinc-dependent MAM binding to LG2 cells can be abolished by addition of EDTA (Etongue-Mayer et al., 2002). It has been speculated that zinc-dependent MAM binding to LG2 cells results from a direct involvement of zinc in the interactions between MAM and the class II MHC molecule HLA-DR1, since MAM binding to LG2 cells was completely inhibited by the presence of anti-HLA-DR mAb, whereas the anti-HLA-DP, anti-HLA-DQ, anti-CD40, or anti-MHC class I mAbs had no effect (Etongue-Mayer et al., 2002). Alternatively, zinc could be involved in the formation of a MAM homodimer, which may be required for the protein’s biological function (Langlois et al., 2003). Indeed, our recent structural study revealed that MAM forms an asymmetric homodimer that can cross-link two MHC molecules (Zhao et al., 2004a). However, zinc was found neither at the MAM dimer interface nor at the MAM-MHC interface in the crystal (Zhao et al., 2004a).

To characterize this unique SAg MAM, we used biochemical, biophysical, and mutagenetic approaches to study MAM dimerization in solution. Our results show that, although MAM mainly exist as a monomer in solution, a small proportion of MAM forms homodimer at high concentration in solution, independent of variations in buffer conditions. Distinct peaks corresponding to the MAM homodimer were detected in the presence of EDTA using both chemical cross-linking and AUC methods, implying that Zn^{2+} is not directly involved in MAM dimerization. Our results differs from that of a previous study (Langlois et al., 2003) in which a Zn^{2+}-dependent MAM dimer was seen using a chemical cross-linking method,

with a cross-linker bismaleimidohexane (BMH) that requires free-cysteines for reaction. This discrepancy might result from the use of a different cross-linker and/or different methods. Our combined chemical cross-linking, AUC, and crystallographic results suggested to us that MAM can form a weak dimer, regardless of the presence of Zn^{2+}.

To further characterize MAM dimerization, we performed mutagenesis on MAM residues that occur at the dimer interface of MAM in the MAM/HLA-DR1/HA co-crystal structure (Zhao et al., 2004a). Several interesting findings were obtained. Of the nine amino acids selected for mutation to alanines, four mutants, H58A, Y193A, Y194A, and D197A, gave very poor protein yields compared to MAM_{wt}. It is possible that these residues play critical roles in maintaining the structural stability of MAM. Y193 and Y194 are located on a hydrophobic surface formed by residues L146, I190, L200, and F211, while H58 forms one hydrogen bond with D115, which is near the interface between the N- and C-terminal domains, and D197 forms hydrogen bonds with the side-chain of R192 and the main-chain amide nitrogen of E199 (Zhao et al., 2004a). Mutation of any of these four residues could reduce local structural stability, leading to protein misfolding. Alternatively, these residues may be important for MAM dimerization, which in turn may be essential to stabilize MAM structure. However, such a conclusion is speculative, because MAM shows only a very weak tendency to dimerize, with a K_D in millimolar range. Sedimentation studies of five other MAM mutants, L50A, R154A, R192A, E195A, and K201A, revealed that these mutations do not significantly affect the dimerization of MAM in solution. The mutagenesis and sedimentation data could imply that these mutations are not essential for MAM dimerization. On the other hand, the crystallographic dimer from which these mutations were designed may not be equivalent to the native MAM dimer in solution. Further structural studies of MAM homodimer in unliganded form will be required to definitively determine which residues are involved in MAM native dimer formation, and what roles they play.

To investigate the biophysical properties of MAM and to investigate the role of zinc, we performed CD spectral analysis. Our results indicated that no overall global conformational changes occur at the secondary structural level for MAM, upon addition of excess Zn^{2+}. In addition, addition of Zn^{2+} does not induce conformational changes of MAM from its apo state in tertiary structure level.

Further thermal denaturation studies revealed suggestive findings. Our results indicated that MAM is generally less stable than are the pyrogenic bacterial SAgs, which are characterized by their high structural stability. The T_m was determined as over 55 °C for representative bacterial SAgs, *Staphylococcus* enterotoxins (SEs) A, B, and H, in the presence of EDTA (Cavallin et al., 2000; Cavallin et al., 2003); the T_m for apo MAM is at least 6 °C lower. Addition of excess EDTA to the MAM solution did not change the melting curve, relative to that for apo-MAM, and it produced a nearly identical value for the T_m. In contrast, addition of excess Zn^{2+} to the MAM solution strongly modified the melting curve. Addition of Zn^{2+} did not result in a T_m increase, but instead a T_m decrease of nearly 4.7 °C, from the T_m of MAM in apo state (Fig. 4C). Upon addition of zinc, a T_m decrease up to 3.2 °C has also been observed for the SAg SEB (Cavallin et al., 2003). It is believed that coordination of metal ions often leads to stabilization of structures, since increases in melting point T_m of approximately 10 °C have been measured (Burlacu-Miron et al., 1998; Kanaya et al., 1996). For instance, addition of Zn^{2+} resulted in T_m increases for SEA and SEH, implying that both SEA and SEH are stabilized by addition of Zn^{2+}. Zn^{2+} is known to play critical roles in SEA and SEH function through its direct involvement in interactions between SEA/H and the MHC molecules. In contrast, the opposite effect, a decrease in T_m, was seen for SEB (Cavallin et al., 2003) and MAM. The T_m decrease for SEB is consistent with the fact that the biological function of SEB is known to be Zn^{2+}-independent. For MAM, the T_m

decrease upon addition of zinc similarly implies that there is no defined Zn^{2+}-binding site on MAM. Consistently, we did not find zinc ions in the crystal structure of the MAM-MHC complex, even though crystals were grown in the presence of excess Zn^{2+} (Zhao et al., 2004a).

In conclusion, we have used biochemical, biophysical, and mutagenetic approaches to investigate MAM dimerization in solution. We demonstrated that MAM can form a Zn^{2+}-independent homodimer in solution, and that Zn^{2+} does not induce conformational changes of MAM. Further studies will be required to address whether Zn^{2+} play other roles, such as in interaction with co-stimulatory receptors and/or in induction of receptor dimerization, in MAM-mediated T-cell activation.

Acknowledgments

This work was supported by NIH (NIAID) Grant R01 AI50628 (to H.M.L.). W.M. was supported by grants from the Arthritis Society of Canada, the Canadian Arthritis Network, and the Canadian Institutes of Health Research. We thank the Biochemistry Core facility at the Wadsworth Center for assistance with sedimentation and CD experiments, and the Molecular Genetics Core facility for DNA sequencing. We thank A. Verschoor and D. LeMaster at the Wadsworth Center for a critical reading and valuable discussion of the manuscript.

Abbreviations

MAM	*Mycoplasma arthritidis*-derived mitogen
SAg	superantigen
TCR	T-cell receptor
EDTA	ethylendiaminetetraacetic acid
CD	circular dichroism
T_m	melting point
MHC	major histocompatibility complex
HA	haemagglutinin peptide 306–318
APC	antigen-presenting cell
DSG	disuccinimidyl glutarate
DMSO	dimethyl sulfoxide
SV	sedimentation velocity
AUC	analytical ultracentrifuge
HBS	Hepes-buffered saline
$S_{(20,w)}$	sedimentation coefficient
K_D	dissociation constant

References

Abe J, Kotzin BL, Jujo K, Melish ME, Glode MP, Kohsaka T, Leung DY. Selective expansion of T cells expressing T-cell receptor variable regions V beta 2 and V beta 8 in Kawasaki disease. Proc Natl Acad Sci USA. 1992; 89:4066–4070. [PubMed: 1315049]

Acharya KR, Passalacqua EF, Jones EY, Harlos K, Stuart DI, Brehm RD, Tranter HS. Structural basis of superantigen action inferred from crystal structure of toxic-shock syndrome toxin-1. Nature. 1994; 367:94–97. [PubMed: 8107781]

Adler AJ, Greenfield NJ, Fasman GD. Circular dichroism and optical rotatory dispersion of proteins and polypeptides. Methods Enzymol. 1973; 27:675–735. [PubMed: 4797940]

Al-Daccak R, Mehindate K, Damdoumi F, Etongue-Mayer P, Nilsson H, Antonsson P, Sundstrom M, Dohlsten M, Sekaly RP, Mourad W. Staphylococcal enterotoxin D is a promiscuous superantigen offering multiple modes of interactions with the MHC class II receptors. J Immunol. 1998; 160:225–232. [PubMed: 9551975]

Arcus VL, Langley R, Proft T, Fraser JD, Baker EN. The Three-dimensional structure of a superantigen-like protein, SET3, from a pathogenicity island of the Staphylococcus aureus genome. J Biol Chem. 2002; 277:32274–32281. [PubMed: 12082105]

Arcus VL, Proft T, Sigrell JA, Baker HM, Fraser JD, Baker EN. Conservation and variation in superantigen structure and activity highlighted by the three-dimensional structures of two new superantigens from Streptococcus pyogenes. J Mol Biol. 2000; 299:157–168. [PubMed: 10860729]

Baker HM, Proft T, Webb PD, Arcus VL, Fraser JD, Baker EN. Crystallographic and mutational data show that the streptococcal pyrogenic exotoxin J can use a common binding surface for T-cell receptor binding and dimerization. J Biol Chem. 2004a; 279:38571–38576. [PubMed: 15247241]

Baker MD, Gendlina I, Collins CM, Acharya KR. Crystal structure of a dimeric form of streptococcal pyrogenic exotoxin A (SpeA1). Protein Sci. 2004b; 13:2285–2290. [PubMed: 15295110]

Bernatchez C, Al-Daccak R, Mayer PE, Mehindate K, Rink L, Mecheri S, Mourad W. Functional analysis of Mycoplasma arthritidis-derived mitogen interactions with class II molecules. Infect Immun. 1997; 65:2000–2005. [PubMed: 9169724]

Burlacu-Miron S, Perrier V, Gilles AM, Pistotnik E, Craescu CT. Structural and energetic factors of the increased thermal stability in a genetically engineered Escherichia coli adenylate kinase. J Biol Chem. 1998; 273:19102–19107. [PubMed: 9668095]

Cavallin A, Arozenius H, Kristensson K, Antonsson P, Otzen DE, Bjork P, Forsberg G. The spectral and thermodynamic properties of staphylococcal enterotoxin A, E, and variants suggest that structural modifications are important to control their function. J Biol Chem. 2000; 275:1665–1672. [PubMed: 10636860]

Cavallin A, Petersson K, Forsberg G. Spectrophotometric methods for the determination of superantigen structure and stability. Methods Mol Biol. 2003; 214:55–63. [PubMed: 12489454]

Cole BC, Knudtson KL, Oliphant A, Sawitzke AD, Pole A, Manohar M, Benson LS, Ahmed E, Atkin CL. The sequence of the Mycoplasma arthritidis superantigen, MAM: identification of functional domains and comparison with microbial superantigens and plant lectin mitogens. J Exp Med. 1996; 183:1105–1110. [PubMed: 8642252]

Conrad B, Weidmann E, Trucco G, Rudert WA, Behboo R, Ricordi C, Rodriquez-Rilo H, Finegold D, Trucco M. Evidence for superantigen involvement in insulin-dependent diabetes mellitus aetiology. Nature. 1994; 371:351–355. [PubMed: 8090207]

Dam J, Guan R, Natarajan K, Dimasi N, Chlewicki LK, Kranz DM, Schuck P, Margulies DH, Mariuzza RA. Variable MHC class I engagement by Ly49 natural killer cell receptors demonstrated by the crystal structure of Ly49C bound to H-2K(b). Nat Immunol. 2003; 4:1213–1222. [PubMed: 14595439]

Donadini R, Liew CW, Kwan AH, Mackay JP, Fields BA. Crystal and solution structures of a superantigen from Yersinia pseudotuberculosis reveal a jelly-roll fold. Structure (Camb). 2004; 12:145–156. [PubMed: 14725774]

Driessen C, Hirv K, Kirchner H, Rink L. Divergent effects of zinc on different bacterial pathogenic agents. J Infect Dis. 1995; 171:486–489. [PubMed: 7844397]

Etongue-Mayer P, Langlois MA, Ouellette M, Li H, Younes S, Al-Daccak R, Mourad W. Involvement of zinc in the binding of mycoplasma arthritidis-derived mitogen to the proximity of the HLA-DR binding groove regardless of histidine 81 of the beta chain. Eur J Immunol. 2002; 32:50–58. [PubMed: 11754003]

Gemmell E, Grieco DA, Cullinan MP, Westerman B, Seymour GJ. Antigen-specific T-cell receptor V beta expression in Porphyromonas gingivalis-specific T-cell lines. Oral Microbiol Immunol. 1998; 13:355–361. [PubMed: 9872111]

Guan R, Malchiodi EL, Wang Q, Schuck P, Mariuzza RA. Crystal structure of the C-terminal peptidogly can-binding domain of human peptidoglycan recognition protein Ialpha. J Biol Chem. 2004; 279:31873–31882. [PubMed: 15140887]

Hakansson M, Petersson K, Nilsson H, Forsberg G, Bjork P, Antonsson P, Svensson LA. The crystal structure of staphylococcal enterotoxin H: implications for binding properties to MHC class II and TcR molecules. J Mol Biol. 2000; 302:527–537. [PubMed: 10986116]

Hudson KR, Tiedemann RE, Urban RG, Lowe SC, Strominger JL, Fraser JD. Staphylococcal enterotoxin A has two cooperative binding sites on major histocompatibility complex class II. J Exp Med. 1995; 182:711–720. [PubMed: 7650479]

Kanaya S, Oobatake M, Liu Y. Thermal stability of Escherichia coli ribonuclease HI and its active site mutants in the presence and absence of the Mg^{2+} ion. Proposal of a novel catalytic role for Glu48. J Biol Chem. 1996; 271:32729–32736. [PubMed: 8955106]

Kim, MH.; Schlievert, P. Molecular genetics, structure, and immunobiology of streptococcal pyrogenic exotoxins A and C. In: Leung, DYM.; Huber, BT.; Schlievert, PM., editors. Superantigens: Molecular Biology, Immunology, and Relevance to Human Disease. 1997. p. 257-280.

Knudtson KL, Manohar M, Joyner DE, Ahmed EA, Cole BC. Expression of the superantigen Mycoplasma arthritidis mitogen in Escherichia coli and characterization of the recombinant protein. Infect Immun. 1997; 65:4965–4971. [PubMed: 9393783]

Kotzin BL, Leung DY, Kappler J, Marrack P. Superantigens and their potential role in human disease. Adv Immunol. 1993; 54:99–166. [PubMed: 8397479]

Kozono H, Parker D, White J, Marrack P, Kappler J. Multiple binding sites for bacterial superantigens on soluble class II MHC molecules. Immunity. 1995; 3:187–196. [PubMed: 7648392]

Langlois MA, El Fakhry Y, Mourad W. Zinc-binding sites in the N terminus of Mycoplasma arthritidis-derived mitogen permit the dimer formation required for high affinity binding to HLA-DR and for T cell activation. J Biol Chem. 2003; 278:22309–22315. [PubMed: 12676930]

Langlois MA, Etongue-Mayer P, Ouellette M, Mourad W. Binding of Mycoplasma arthritidis-derived mitogen to human MHC class II molecules via its N terminus is modulated by invariant chain expression and its C terminus is required for T cell activation. Eur J Immunol. 2000; 30:1748–1756. [PubMed: 10898513]

Lebowitz J, Lewis MS, Schuck P. Modern analytical ultracentrifugation in protein science: a tutorial review. Protein Sci. 2002; 11:2067. [PubMed: 12192063]

Li H, Llera A, Malchiodi EL, Mariuzza RA. The structural basis of T cell activation by superantigens. Annu Rev Immunol. 1999; 17:435–466. [PubMed: 10358765]

Li PL, Tiedemann RE, Moffat SL, Fraser JD. The superantigen streptococcal pyrogenic exotoxin C (SPE-C) exhibits a novel mode of action. J Exp Med. 1997; 186:375–383. [PubMed: 9236189]

Li Y, Li H, Dimasi N, McCormick JK, Martin R, Schuck P, Schlievert PM, Mariuzza RA. Crystal structure of a superantigen bound to the high-affinity, zinc-dependent site on MHC class II. Immunity. 2001; 14:93–104. [PubMed: 11163233]

Mehindate K, Thibodeau J, Dohlsten M, Kalland T, Sekaly RP, Mourad W. Cross-linking of major histocompatibility complex class II molecules by staphylococcal enterotoxin A superantigen is a requirement for inflammatory cytokine gene expression. J Exp Med. 1995; 182:1573–1577. [PubMed: 7595227]

Mitchell DT, Levitt DG, Schlievert PM, Ohlendorf DH. Structural evidence for the evolution of pyrogenic toxin superantigens. J Mol Evol. 2000; 51:520–531. [PubMed: 11116326]

Papageorgiou AC, Acharya KR, Shapiro R, Passalacqua EF, Brehm RD, Tranter HS. Crystal structure of the superantigen enterotoxin C2 from Staphylococcus aureus reveals a zinc-binding site. Structure. 1995; 3:769–779. [PubMed: 7582894]

Papageorgiou AC, Baker MD, McLeod JD, Goda SK, Manzotti CN, Sansom DM, Tranter HS, Acharya KR. Identification of a secondary zinc-binding site in staphylococcal enterotoxin C2. Implications for superantigen recognition. J Biol Chem. 2004; 279:1297–1303. [PubMed: 14559915]

Papageorgiou AC, Collins CM, Gutman DM, Kline JB, O'Brien SM, Tranter HS, Acharya KR. Structural basis for the recognition of superantigen streptococcal pyrogenic exotoxin A (SpeAl) by MHC class II molecules and T-cell receptors. Embo J. 1999; 18:9–21. [PubMed: 9878045]

Petersson K, Hakansson M, Nilsson H, Forsberg G, Svensson LA, Liljas A, Walse B. Crystal structure of a superantigen bound to MHC class II displays zinc and peptide dependence. Embo J. 2001; 20:3306–3312. [PubMed: 11432818]

Prasad GS, Earhart CA, Murray DL, Novick RP, Schlievert PM, Ohlendorf DH. Structure of toxic shock syndrome toxin 1. Biochemistry. 1993; 32:13761–13766. [PubMed: 8268150]

Renno T, Acha-Orbea H. Superantigens in autoimmune diseases: still more shades of gray. Immunol Rev. 1996; 154:175–191. [PubMed: 9034868]

Roussel A, Anderson BF, Baker HM, Fraser JD, Baker EN. Crystal structure of the streptococcal superantigen SPE-C: dimerization and zinc binding suggest a novel mode of interaction with MHC class II molecules. Nat Struct Biol. 1997; 4:635–643. [PubMed: 9253413]

Sawitzke A, Joyner D, Knudtson K, Mu HH, Cole B. Anti-MAM antibodies in rheumatic disease: evidence for a MAM-like superantigen in rheumatoid arthritis? J Rheumatol. 2000; 27:358–364. [PubMed: 10685797]

Schad EM, Papageorgiou AC, Svensson LA, Acharya KR. A structural and functional comparison of staphylococcal enterotoxins A and C2 reveals remarkable similarity and dissimilarity. J Mol Biol. 1997; 269:270–280. [PubMed: 9191070]

Schuck P, Perugini MA, Gonzales NR, Howlett GJ, Schubert D. Size-distribution analysis of proteins by analytical ultracentrifugation: strategies and application to model systems. Biophys J. 2002; 82:1096–1111. [PubMed: 11806949]

Sreerama N, Woody RW. Estimation of protein secondary structure from circular dichroism spectra: comparison of CONTENT, SELCON, and CDSSTR methods with an expanded reference set. Anal Biochem. 2000; 287:252–260. [PubMed: 11112271]

Sundberg E, Jardetzky TS. Structural basis for HLA-DQ binding by the streptococcal superantigen SSA. Nat Struct Biol. 1999; 6:123–129. [PubMed: 10048922]

Sundberg EJ, Li Y, Mariuzza RA. So many ways of getting in the way: diversity in the molecular architecture of superantigen-dependent T-cell signaling complexes. Curr Opin Immunol. 2002; 14:36–44. [PubMed: 11790531]

Sundstrom M, Abrahmsen L, Antonsson P, Mehindate K, Mourad W, Dohlsten M. The crystal structure of staphylococcal enterotoxin type D reveals Zn^{2+}-mediated homodimerization. Embo J. 1996; 15:6832–6840. [PubMed: 9003758]

Swaminathan S, Furey W, Pletcher J, Sax M. Crystal structure of staphylococcal enterotoxin B, a superantigen. Nature. 1992; 359:801–806. [PubMed: 1436058]

Vistica J, Dam J, Balbo A, Yikilmaz E, Mariuzza RA, Rouault TA, Schuck P. Sedimentation equilibrium analysis of protein interactions with global implicit mass conservation constraints and systematic noise decomposition. Anal Biochem. 2004; 326:234–256. [PubMed: 15003564]

Zhao Y, Li Z, Drozd S, Guo Y, Mourad W, Li H. Crystal structure of Mycoplasma arthritidis mitogen complexed with HLA-DR1 reveals a novel superantigen fold and a dimerized superantigen-MHC complex. Structure. 2004a; 12:277–288. [PubMed: 14962388]

Zhao Y, Li Z, Drozd S, Guo Y, Stack R, Hauer C, Li H. Crystallization and preliminary crystallographic analysis of Mycoplasma arthritidis-derived mitogen complexed with peptide/MHC class II antigen. Acta Crystallogr D Biol Crystallogr. 2004b; 60:353–356. [PubMed: 14747723]

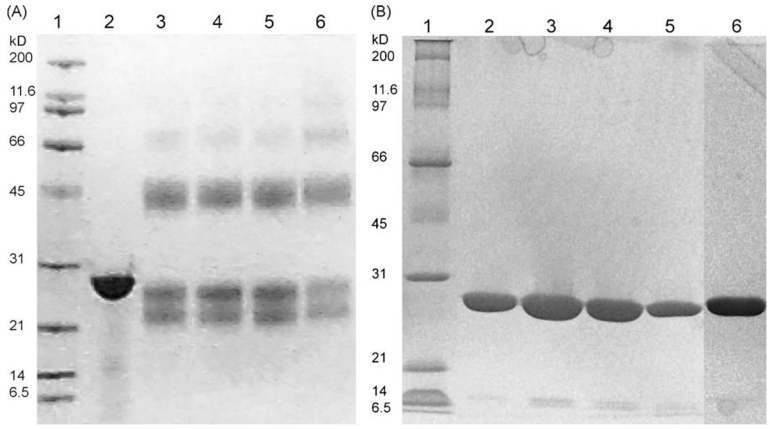

Fig. 1.

SDS-PAGE analysis of MAM dimerization and MAM mutants. (A) SDS-PAGE analysis of recombinant MAM treated with or without DSG, in the presence of Zn^{2+} or EDTA. Lane 1, Bio-Rad broad range molecular weight (MW) standard; lane 2, MAM alone; lanes 3–6, MAM (3 μM) treated with 1 mM DSG, after incubation with 30 μM $Zn(OAc)_2$ (lane 3); with 30 μM EDTA (lane 4); with water (lane 5); or with 300 μM $Zn(OAc)_2$ (lane 6); (B) SDS-PAGE analysis of recombinant MAM mutants, I50A (lane 2), R154A (lane 3), R192A (lane 4), E195A (lane 5), and K201A (lane 6). Lane 1, Bio-rad broad range MW standard.

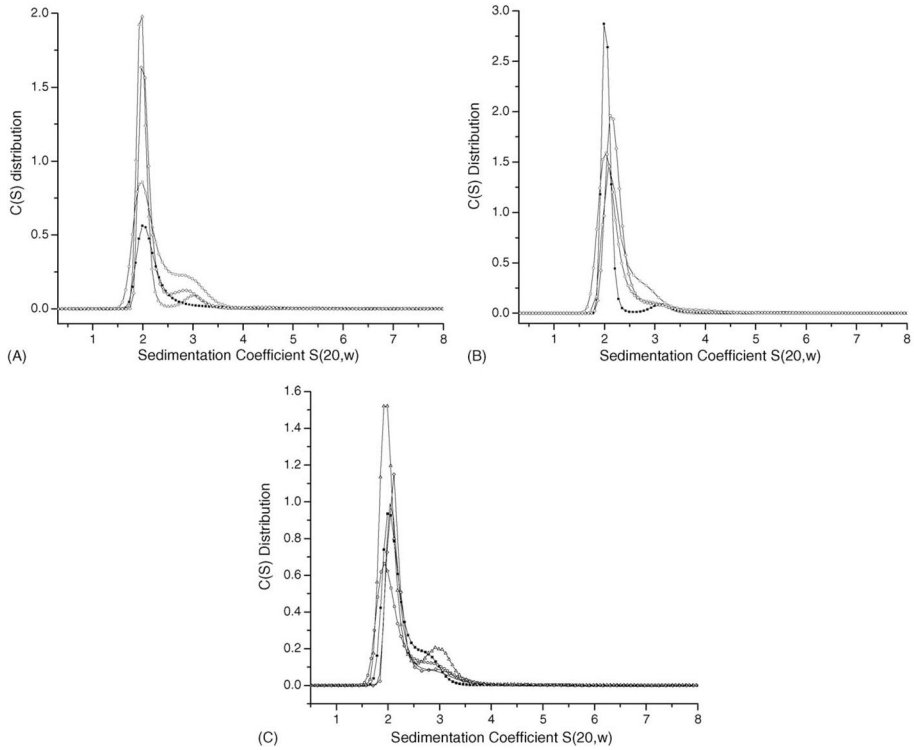

Fig. 2.

Sedimentation velocity analysis of MAM dimerization. (A) Sedimentation coefficient distributions of MAM_{wt} at concentrations of 11 μM (-■ -), 25 μM (-△ -), and 52 μM (-○ -) in buffer A, and at a concentration of 45 μM in buffer A supplemented with 5 mM EDTA (-◇ -); (B) Sedimentation coefficient distributions of MAM_{wt} at 62 μM in citrate buffer (-■ -), at 55 μM in the Tris-HCl buffer (-□ -), at 55 μM in the HBS buffer (-◇ -), or at 27 μM in buffer A supplemented with 2 mM $ZnCl_2$ (-○ -); (C) Sedimentation coefficient distributions of MAM mutants I50A (11 μM) (-■ -), R154A (70 μM) (-◇ -), R192A (70 μM) (—), E195A (50 μM) (-○ -), K201A (42 μM) (-△ -) in buffer A.

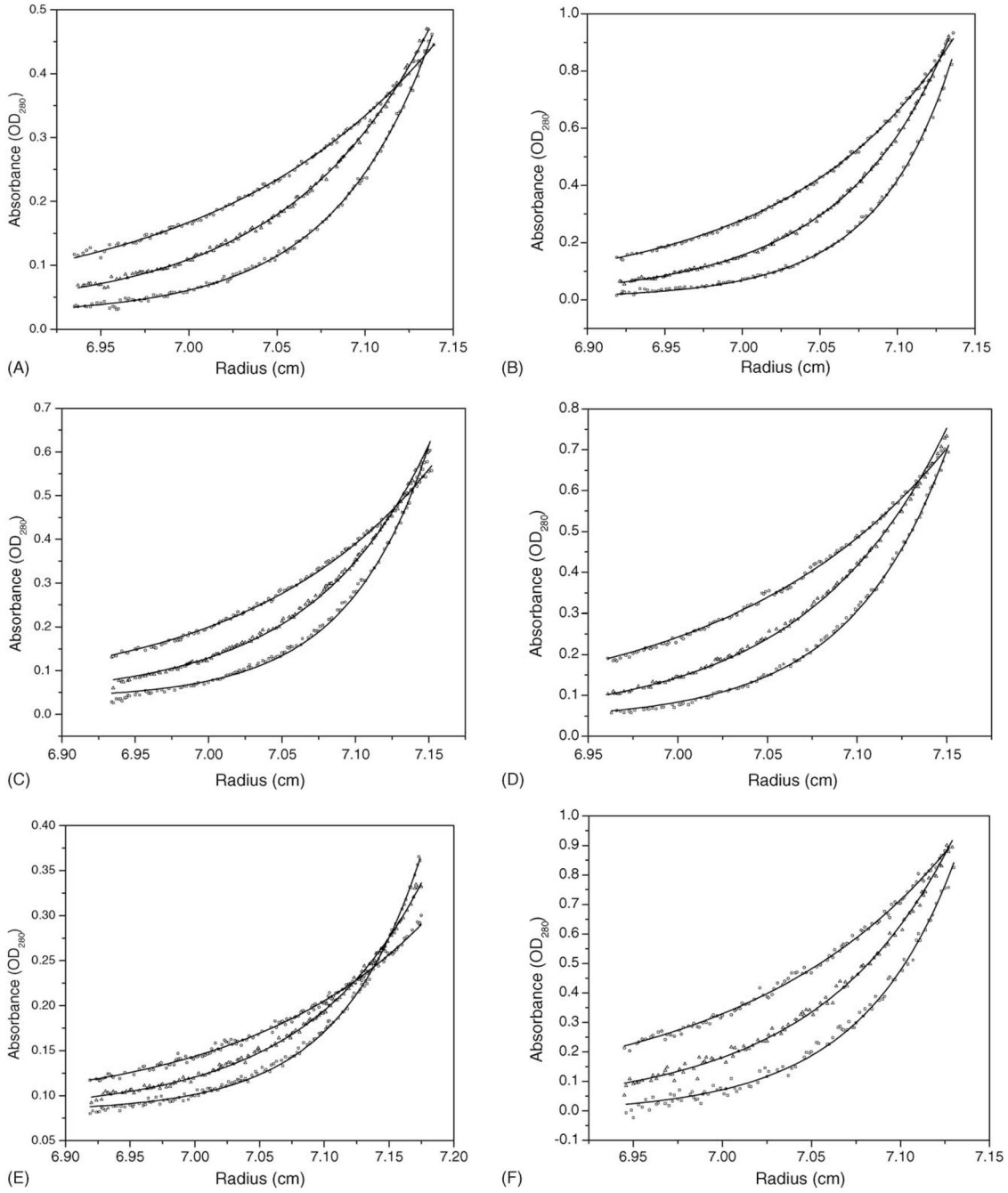

Fig. 3.

Sedimentation equilibrium analysis of MAM_{wt} and MAM mutants. Representative absorbance distributions for the sedimentation of MAM_{wt} at 10 μM (panel A), and of MAM mutants I50A at 20 μM (panel B), R154A at 20 μM (panel C), R192A at 20 μM (panel D), E195A at 14 μM (panel E), K201A at 39 μM (panel F), at 20 °C at rotor speeds of 20,000 rpm (circles), 25,000 rpm (triangles), and 30,000 rpm (squares). Distributions were analyzed as part of a global fitting to the absorbance data at multiple loading concentrations. *Solid lines* are the global best-fit distributions using a reversible monomer-dimer model.

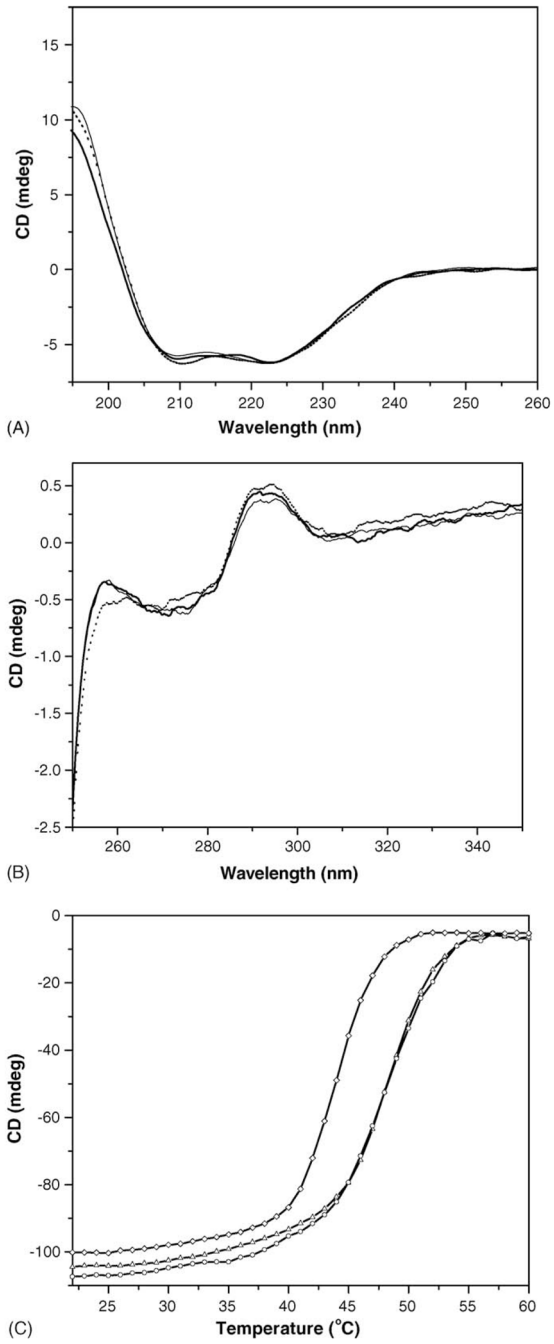

Fig. 4.

CD spectra of MAM in the presence of exces EDTA, excess Zn^{2+}, or in buffer alone. (A) Far-UV CD spectra of MAM in the HBS buffer (thick line —) or supplemented with 1 mM EDTA (thin line —) or 1 mM $ZnCl_2$ (dotted line…). (B) Near-UV CD spectra of MAM in HBS buffer (thick line —) or supplemented with 1 mM EDTA (thin line —) or 1 mM $ZnCl_2$ (dotted line…); (C) Temperature dependence of molar ellipticity at 222 nm for MAM HBS buffer (-○ -) or supplemented with 1 mM EDTA (-△ -) or 1 mM $ZnCl_2$ (-◇ -).